Characterisation of the metabolome of ocular tissues and postmortem changes in the rat retina

DOI:
10.1016/j.exer.2016.05.019

Document Version
Accepted author manuscript

Characterisation of the metabolome of ocular tissues and post-mortem changes in the rat retina

Shi Z. Tan[1,3],‡ Graham Mullard[2,4], Katherine A. Hollywood[2,4,6], Warwick B. Dunn[5,‡] and Paul N. Bishop [1,3,4,]

[1] Centre for Ophthalmology and Vision Sciences and [2] Centre for Endocrinology and Diabetes, Institute of Human Development, Faculty of Medical and Human Sciences, University of Manchester, Manchester, M13 9PL, UK.
[3] Manchester Royal Eye Hospital and [4] Centre for Advanced Discovery and Experimental Therapeutics (CADET), Central Manchester University Hospitals NHS Foundation Trust, Manchester Academic Health Science Centre, Manchester, M13 9WL, UK
[5] School of Biosciences and Phenome Centre Birmingham, University of Birmingham, Edgbaston, Birmingham, B15 2TT, UK.
[6] Faculty of Life Science, University of Manchester, Manchester, M13 9PL, UK.

‡ Corresponding author:
Dr Shi Zhuan Tan
Email: shizhuan@gmail.com
Phone: +44 (0)161 276 1234
Fax: +44 (0)161 701 0242

Abstract

Time-dependent post-mortem biochemical changes have been demonstrated in donor cornea and vitreous, but there have been no published studies to date that objectively measure post-mortem changes in the retinal metabolome over time. The aim of the study was firstly, to investigate post-mortem, time-dependent changes in the rat retinal metabolome and secondly, to compare the metabolite composition of healthy rat ocular tissues. To study post-mortem changes in the rat retinal metabolome, globes were enucleated and stored at 4^{o}C and sampled at 0, 2, 4, 8, 24 and 48 hours post-mortem. To study the metabolite composition of rat ocular tissues, eyes were dissected immediately after culling to isolate the cornea, lens, vitreous and retina, prior to storing at –80^{o}C. Tissue extracts were subjected to Gas Chromatograph Mass Spectrometry (GC-MS) and Ultra High Performance Liquid Chromatography Mass Spectrometry (UHPLC-MS). Generally, the metabolic composition of the retina was stable for 8 hours post-mortem when eyes were stored at 4^{o}C, but showed increasing changes thereafter. However, some more rapid changes were observed such as increases in TCA cycle metabolites after 2 hours post-mortem, whereas some metabolites such as fatty acids only showed decreases in concentration from 24 hours. A total of 42 metabolites were identified across the ocular tissues by GC-MS (MSI level 1) and 2782 metabolites were annotated by UHPLC-MS (MSI level 2) according to MSI reporting standards. Many of the metabolites detected were common to all of the tissues but some metabolites showed partitioning between different ocular structures with 655, 297, 93 and 13 metabolites being uniquely detected in the retina, lens, cornea and vitreous respectively. Only a small percentage (1.6%) of metabolites found in the vitreous were exclusively found in the retina and not other tissues. In conclusion, mass

spectrometry-based techniques have been used for the first time to compare the metabolic composition of different ocular tissues. The metabolite composition of the retina of eyes kept at 4^{o}C post-mortem is mostly stable for at least 8 hours.

INTRODUCTION

Metabolites have many important roles in biological systems.[1] The total complement of metabolites in a biological system is defined as the metabolome; its composition is both sample- and time-dependent.[2, 3] As metabolites are the end product of biological pathways, the metabolome is a sensitive measure of disease phenotype and a dynamic indicator of genetic, environmental or disease-specific perturbations.[1,4, 5]

Metabolomics is increasingly being applied as a tool in eye research. It has been used to characterise normal ocular tissues and biofluids including the tear film, lens, vitreous and retina.[6-10] It has also been used to study ageing, a variety of ocular pathologies, metabolite transport in the retina, effects of drugs and metabolic changes during corneal organ culture for transplantation.[11-15]

Aqueous and vitreous are the most accessible intraocular samples that can be obtained in clinical studies, and these have been used to interrogate the metabolic activities of surrounding ocular structures.[11, 15] However, it is unclear whether sampling ocular biofluids provides robust and reproducible information on the metabolic activity of surrounding tissues and ideally, the metabolome of the ocular tissue of interest should be studied directly. One option is to use post-mortem eyes. However, a concern with this approach is that the concentration of metabolites can alter rapidly post-mortem caused by continued metabolic activity or metabolite instability. Time-dependent post-mortem biochemical changes have been demonstrated in donor cornea[16] and vitreous[17], but to the best of our knowledge, there have been no published studies to date that objectively measure post-mortem changes in the retinal metabolome over time. This is important baseline information for future study design.

The objectives of the study reported here were (1) to investigate post-mortem changes in the rat retinal metabolome over 48 hours when eyes are stored at 4^{o}C (temperature at which human post-mortem eyes are stored in real-life) and (2) for the first time, annotate and characterise the metabolic composition of four ocular tissues (cornea, lens, vitreous and retina).

METHODS

Animals

All animal experiments were conducted in accordance with the United Kingdom (UK) Home Office regulations for the care and use of laboratory animals, the UK Animals (Scientific Procedures) Act (1986), and the ARVO Statement for the Use of Animals in Ophthalmic and Vision Research. Twenty-one, male, Sprague Dawley rats were included in the post-mortem study (42 eyes in total) and six rats were included in the tissue comparison study; all rats were in the age-range of 7-12 weeks. The rats were kept in the same room under standard laboratory conditions and fed with standard chow. The rats were culled by carbon dioxide inhalation followed by cervical extension; this process was staggered to ensure rapid sample collection. Enucleation was performed as soon as possible (between 1 to 20 minutes) after death. If eyes were not dissected immediately (T=0 hour samples), they were placed in small bottles and stored on ice before transferring to a refrigerator and then stored in the dark for up to 48 hours at 4°C (T=2-48 hour samples).

Dissection

Seven eyes were studied at each time point for the retinal metabolic stability study and six eyes were studied to annotate and characterise the metabolome of

different ocular tissues. Dissections of the rat eyes at T=0 were performed immediately after culling and the stored eyes were dissected at 2, 4, 8, 12, 24 and 48 hours post culling to remove the retina. Under microscope guidance the cornea was carefully removed. Then the iris was divided with forceps and the lens removed in one piece to gain access to the posterior segment. Vitreous was meticulously separated from the retina. Lastly, the neurosensory retina was removed avoiding contamination with the retinal pigment epithelium/Bruch's membrane/choroid complex. All dissections were performed on a cold plate to maintain a temperature of approximately 4^{o}C and dissection time was between 2 to 5 minutes. The dissected tissues were snap-frozen with liquid nitrogen and then stored at -80^{o}C before extraction.

Sample preparation

Each tissue sample was carefully weighed prior to extraction, mean weights were as follows; retina 25.4mg; vitreous 30.1mg; lens 32.7mg; cornea 7.9mg. Metabolite extraction was achieved by adding 800µL of chloroform:methanol (50:50, pre-cooled to -20^{o}C) followed by 50µL of an internal standard mixture (0.1 mg/ml d_5 Benzoic acid, d_4 Succinic acid and d_5 Glycine dissolved in methanol) to each pre-weighed sample. Homogenisation/extraction was performed in a TissueLyser (Qiagen; 25Hz, 10 minutes using one 3mm tungsten carbide bead). Next, 400µL of water was added and the mixture was vortexed and allowed to stand on ice for 10 minutes. The samples were then centrifuged (5 minutes, 13,000*g*) to allow separation of the solvents. The top hydrophilic layer (to be analysed by GC-MS) and bottom lipophilic layer (to be used for UHPLC-MS analysis) were transferred into separate tubes and dried (Savant SPD131DDA with an RVT4104 cold trap, Thermo Scientific).

The volume of polar and non-polar extractions collected was normalised to the lowest tissue weight for each tissue type in each study. Quality control (QC) samples were prepared by pooling together an aliquot of 100µL from each retina sample after extraction and before drying. The QC samples were used for quality assurance as described by Dunn et al.[18]

UHPLC-MS analysis

All tissue extract samples and QC samples were reconstituted in 200µL 50:50 water:methanol prior to analysis. The samples were analysed using an Accela Ultra High Performance Liquid Chromatography system coupled to an electrospray hybrid LTQ-Orbitrap Velos mass spectrometer (ThermoFisher Scientific, Bremen, Germany). All samples were analysed separately in positive and negative ion modes. QC samples were analysed for the first ten injections and then every fifth injection. The last two injections were also QC samples. Chromatographic separations were performed, following injection of a 10µL sample volume, onto a Hypersil GOLD column (100x2.1mm, 1.9µm; ThermoFisher Scientific, Runcorn, UK) with the column temperature set at 50°C. The two solvents applied were solvent A -0.1% formic acid in water (vol/vol) and solvent B -0.1% formic acid in methanol (vol/vol)) at a flow rate of 400µL/min. Solvent A was held at 100% for 0.5 minutes followed by an increase to 100% solvent B over 4.5 minutes, which was then held at 100% solvent B for a further 5.5 minutes. At 10.5 minutes, it was changed to 100% solvent A and held at 100% solvent A to equilibrate for 1.5 minutes. All column eluent was transferred to the mass spectrometer. Full-scan profiling data were acquired in an Orbitrap mass analyser (mass resolution 30,000 at *m/z* =400).

Raw data files (.RAW format) generated from the UHPLC-MS system were converted to the NetCDF format using the File converter program in the XCalibur software package (ThemoFisher Scientific, Bremen, Germany). Deconvolution was performed using XCMS software[19] as described previously.[20] Whilst relative concentrations were measured no absolute quantification of metabolites to define concentrations per gram of tissue was performed. For quality assurance, only metabolite features detected in greater than 60% of QC samples and with a response not deviating greater than 20% from the QC mean were retained for further data analysis. All data was normalised to total peak area for each sample[18]. Annotation of the metabolite features detected in the UHPLC-MS system was performed by applying the PUTMEDID-LCMS set of workflows, as described previously.[21] A retention time window of 3s and a mass error of +/-5ppm was applied with a correlation coefficient of 0.75. Using this technique metabolites were putatively annotated (class 2 annotations) applying mass-to-charge ratio or mass-to-charge ratio and match to MS/MS spectra available in external mass spectral libraries (METLIN, MassBank and mzCloud) according to the Metabolomics Standards Initiative recommendations.[22]

GC-MS analysis

All samples were chemically derivatised prior to analysis. 60µL of a 20mg/mL methoxylamine hydrochloride in dry pyridine solution was added to each sample. The samples were vortex mixed for 10s and heated for 20 minutes at 80°C. 60µL of N-methyl-N-trimethylsilyl-trifluoroacetamide was added and the samples were heated at 80°C for 20 minutes. After cooling, 20µL of a retention marker solution (n-alkanes C_{10}, C_{12}, C_{15}, C_{19}, C_{22}, C_{26}, C_{28}, C_{30}, $C_{32,}$ 3mg/mL in dry pyridine) was added to each solution. The samples were vortex-mixed and centrifuged (15

minutes, 13,000*g*). 96µL of supernatant from each sample was transferred to GC vials for analysis.

All samples were analysed using an Agilent 7890 Gas Chromatograph (Agilent technologies, Stockport, UK) coupled with a LECO Pegasus HT TOF mass spectrometer (Leco, Stockport, UK). QC samples were analysed for the first five injections and then every fifth injection. The last two injections were also QC samples. 1µL pulsed splitless injections were made at 270^{o}C with a Gerstel MPS2 autosampler, using a 30s pressure pulse and purge time, and a 'hot, empty needle' technique, onto a 30mx0.25mmx0.25µm RXi-17 column (Restek) coupled to a 2mx0.25mm intermediate polarity retention gap (Restek), through an Agilent Split/Splitless injector equipped with a 4mm splitless liner. Helium carrier gas was set at a 1.4 mL/min constant flow; oven temperature programme was held at 50^{o}C for 4 minutes, then a linear temperature ramp from 50-150^{o}C at 20^{o}C/min, followed by a linear temperature ramp of 150-300^{o}C at 15^{o}C/min with a hold temperature of 300^{o}C for 4 minutes. The column was led directly into the ion source (220^{o}C) of the mass spectrometer via a transfer line held at 240^{o}C. Data were acquired at 20Hz, over the *m/z* range 45-600Da, with a 420s solvent delay prior to acquisition.

Raw instrument data were pre-processed applying the ChromaTof software (LECO; v4.22) using a previously described method and its associated chromatographic de-convolution algorithm, with the baseline set at 1.0, data point averaging of 3 and average peak width of 2.5.[18] The peak area was reported and the response ratio relative to the internal standard (peak area-metabolite/peak area-succinic-d_4 acid internal standard) was calculated. Whilst relative concentrations were measured no absolute quantification of metabolites to define concentrations per gram of tissue was performed. These data representing normalised peak lists were exported in .txt

format. Most metabolites were definitively identified (MSI level 1), but a small number were putatively annotated (MSI level 2 or 3) according to The Metabolomics Standards Initiative reporting standards[22] by comparison of retention index and mass spectra acquired from the samples with those present in mass spectral libraries (NIST08, Golm Metabolome Database and Manchester Metabolomics Database).[21] Processed data were directly exported to Microsoft Excel® (.xls) worksheets for further data analysis.

Statistical analysis of retina stability

All statistical analyses were carried out using MetaboAnalyst.[23] All data were normalised to total peak area for each sample. Log_2 transformation was applied for univariate analysis to enhance a normal distribution in the datasets. KNN missing value imputation and Pareto scaling was applied for multivariate analysis only. Metabolite features with greater than 50% missing values for the retinal stability study were removed prior to analysis. Univariate analysis applying one-way ANOVA and multivariate analysis (applying Principal Components Analysis (PCA)) were applied to data acquired from both studies. False discovery rate (FDR) was calculated applying the Benjamini–Hochberg procedure,[24] $q<0.05$ was used to determine the statistical significance. FDR applies a statistical approach to correct for multiple testing in large datasets and to control the expected number of false positives.

Comparison of the metabolome of different ocular tissues

Six biological replicates for each tissue type were analysed by applying GC-MS and UHPLC-MS and the metabolites were putatively annotated or identified as described above. For putatively annotated metabolites reported more than once (as

multiple metabolite features with the same retention time but different mass-to-charge ratios) the entry with the highest total peak area sum across all four tissue types was retained while all other duplicates were deleted. Applying this dataset of unique metabolite annotations, the number of metabolites observed in each combination of tissue type was calculated.

Results

1. Post-mortem change in the rat retina metabolome

All data analysis used relative peak areas. The absolute concentrations for all metabolites were not determined as this is not technically feasible for the thousands of metabolites detected in non-targeted metabolomics studies where the metabolome composition is not known prior to data acquisition, as many metabolites are not available to prepare calibration solutions.

Unsupervised multivariate PCA analysis scores plots of the GC-MS data (Figure 1) and the UHPLC-MS data (Figure 2) showed no separation of retinal samples for eyes stored for 0, 2, 4 and 8 hours, whereas samples stored for 24 and 48 hours were clearly separated. These results imply that samples stored at 4°C are largely metabolically stable for the first 8hrs, but that multiple changes in the metabolic composition commence after that.

Univariate one-way ANOVA was applied to identify those metabolite features that demonstrated a statistically significant difference in relative concentrations between these time points. 16 identified and 133 annotated metabolite features were statistically significant ($q<0.05$) for GC-MS and UHPLC-MS, respectively. Analysis of the GC-MS data revealed increases in the concentration of two metabolites present

in the TCA cycle from 2 hours post mortem (namely citrate and malate), increases in six and a decrease in one amino acid from 8 hours post mortem and decreased levels of five fatty acids from 24 hours post mortem. (Table 1) More detailed information on these data is available in Supplementary Information 1. Analysis of metabolites detected by UHPLC-MS showed that 10 classes of metabolites underwent statistically significant ($q<0.05$) changes post mortem including acyl carnitines (10), diacylglycerides (12), aromatic amino acids (3), bile acids (7), ceramides and sphingolipids (9), fatty acids/fatty alcohols/fatty amides (16), glycerophospholipids (33), lysoglycerophospholipids (18), steroid hormones (5) and vitamin D metabolites (7). These data are available in Supplementary Information 2. As observed for GC-MS, different metabolites and metabolite classes showed different periods of stability. For example, acyl carnitines showed a change in concentration from as early as two hours, bile acids from 4 hours and aromatic amino acids from 24 hours. Some classes showed that metabolites within each class showed different levels of stability. Box and whisker plots for 4 exemplar metabolites are shown in Figure 3.

2. Characterisation of rat cornea, lens, vitreous and retina metabolome

2.1 GC-MS

A total of 42 unique metabolites were identified according to MSI reporting level 1 (i.e. identified metabolites). 20 were detected in the cornea, 32 in the lens, 19 in the vitreous and 21 in the retina. 1, 13, 2 and 3 unique metabolites were detected only in the cornea, lens, vitreous or retina, respectively. The metabolites may have been present at concentrations lower than the detection limits of the analytical methods applied and therefore this method qualitatively defines differences in

concentrations and not necessarily the presence or absence of a metabolite at any concentration. (See Table 2 for the list of metabolites detected in the tissues.)

2.2 UHPLC-MS

There were a total of 2782 unique metabolites detected in one or more tissue (cornea, lens, vitreous and retina). The majority of metabolites are annotated according to MSI level 2 (i.e. putatively annotated compounds). Many of these were detected in all or most of the tissues with 443 metabolites being common to all tissues. 93, 297, 13 and 655 metabolites were found only in cornea, lens, vitreous and retina respectively. Only 13 of 1261 (1%) metabolites detected in vitreous were unique to vitreous, whereas 655 of 1942 (34%) of metabolites detected in retina were unique to retina. 1.6% of metabolites found in the vitreous were uniquely found in the retina and not other tissues. The list of metabolites detected in the tissues studied can be found in Supplementary Information 3. The Venn diagram in Figure 4 illustrates the distribution of these metabolites across the four tissues. As can be seen a large list of putatively annotated metabolites were detected in one or more tissue. The aim of this study was not to provide a list of all metabolites in each tissue but rather to provide an overview of the similarities and differences in the metabolomes across the four different ocular tissues. Many different classes of metabolites were detected including acyl carnitines, acyl glycerides, amino acids, ceramides and sphingolipids, fatty acids, fatty amides, glycerophospholipids, lysoglycerophospholipids, iodo- and fluoro-metabolites, nucleosides/nucleotides, oxidative phosphorylation, steroid hormones and vitamin D metabolites.

Discussion

Two complementary MS techniques where used in this study: GC-MS that detects small polar metabolites, and UHPLC-MS that detects non-polar metabolites, specifically lipids. The analysis of post-mortem changes in the rat eye was undertaken to establish protocols for the metabolomic analysis of eye tissue from animal models and to explore whether it may be feasible to use human ocular tissue for metabolic studies and if so how quickly it would need to be processed. Univariate and multivariate analysis of data acquired applying GC-MS and UHPLC-MS demonstrated that the metabolic composition of the rat retina remained largely stable for the first 8 hours post-mortem when maintained at 4^{o}C, but thereafter an increasing proportion of metabolites changed in relative concentration. A small number of metabolites showed changes in their concentration from 2 hours, including two metabolites present in the TCA cycle. These metabolites (citrate and malate) increased in concentration, suggesting a reduction in their catabolism and/or an increase in their synthesis. Citrate and malate can be both the substrates and products of the TCA cycle. The TCA cycle consists of sequential reversible, and irreversible chemical reactions, in which its directionality depends on the state of oxygen in the tissue.[25] In anaerobic conditions, oxaloacetate can be converted into malate and this may explain the increased in concentration in our post-mortem retina.[26, 27] In fact, malate has been found to increase 4-fold in cardiac ischaemia.[28] Citrate is used as a substrate only in aerobic conditions towards the synthesis of alpha-ketaglutarate. In anaerobic conditions, backflux may occur and citrate accumulates as a product of the cycle.[29, 30] If the theory of increase in synthesis were true to account for the increased concentration of these 2 metabolites, it suggests that TCA cycle continues in anaerobic condition over 48 hours in the rat retina when

stored at 4^{O}C. An earlier study showed that post-mortem retinas can retain their metabolic capacities for 4- 4 1/2 hours following death and this capacity is increased when the tissue is kept at 4^{o}C[31] but to the best of our knowledge, there are no studies that look at the TCA cycle in post-mortem rat retina. However, it is also likely the increased in concentration of citrate and malate is a result of reduced TCA cycle and hence, reduced consumption of the metabolites. Other metabolites such as the amino acids (leucine, methionine, phenylalanine, tryptophan) were largely stable in the first 24 hours post-mortem but followed an increasing trend over the 48hrs time period. Many of the neurotransmitters required for normal retinal cell function occur as free amino acids in the retina. Most of them are generated from the intermediates in the TCA cycle[32] , suggesting that the TCA cycle is on-going during this period but consumption of the metabolites by the retinal cells may be reduced due to an overall decrease in metabolic activity in hypoxic conditions, hence the increased in its concentration. Further studies are required to investigate other metabolites involved in the TCA cycle under different temperatures.

The level of glutamate, on the other hand, falls over post-mortem time. Glutamate is an excitatory neurotransmitter in the brain and retina. Studies have shown an increased extracellular level of glutamate in cerebral ischaemia.[33, 34] An elevated glutamate level was also found in the vitreous of eyes with glaucoma, thought to be indicative of retinal ganglion cell death.[35] It is uncertain why the glutamate level in our study decreases over post-mortem time where severe hypoxia can be assumed. It may be that the equilibrium favours the synthesis of alpha-ketaglutarate from glutamate in the TCA cycle in the state of hypoxia when the temperature is low.

Uracil, a nucleobase in the nucleic acid of RNA was also found increase in concentration. Similar trend was observed in post-mortem porcine vitreous humour.[36] Ascorbic acid and some of the fatty acids decreased in concentration over time. This is most likely due to an overall reduced synthesis and increased consumption. Ascorbic acid is an antioxidant and it is unsurprising that the level plummets in hypoxic conditions. It should be noted that samples were collected within 20 minutes of death and that a small level of metabolic activity could remain present during this time. This implies that the T=0 samples are potentially not identical to the metabolome at death; however, the authors believe that these changes will be small compared to the metabolic changes observed at later time points. Based upon these experiments we conclude that post-mortem human tissue would need stabilisation within 8 hours following enucleation and storage at $4^{O}C$ to be used for metabolomics studies and that tissue retrieved following surgery could be used if appropriate protocols are in place to quickly stabilise it for metabolomics studies.

A large number of metabolites were identified (to MSI level 1) or annotated (to MSI level 2) in the cornea, lens, vitreous and retina using MS-based techniques; 42 and 2782 for GC-MS and UHPLC-MS respectively. We decided to analyse the water-soluble metabolites applying GC-MS though the application of UHPLC-MS applying a HILIC column would allow a greater number of water-soluble metabolites to be detected. The data acquired show that some identified/annotated metabolites were uniquely detected in only one tissue, whereas many others were detected in two or more tissues. The retina displayed the most unique profile of identified/annotated metabolites with 655 detected only in this tissue. The cornea and vitreous contained

fewer unique identified/annotated metabolites. Interestingly, only a small percentage (1.6%) of identified/annotated metabolites found in the vitreous were exclusively found in the retina and not other tissues. Vitreous is composed of approximately 98% water, 1% macromolecules including collagen, hyaluronan and soluble protein and low molecular weight molecules including metabolites that are derived from adjacent ocular tissues and blood plasma.[37] There is metabolic exchange between the cornea and aqueous, and the lens with vitreous and aqueous; so the movement of metabolites between these compartments may explain the similarities between the metabolites found in the lens, vitreous and cornea. However, there is a bulk flow of water posteriorly from the vitreous through the retina[38] and this uni-directional anterior to posterior flow may inhibit the anterior movement of small molecules from the retina into the vitreous resulting in the vitreous metabolome not reflecting that of the retina. Vitreous has been used as the surrogate for analysing molecular changes taking place in the retina, but this study suggests that metabolic footprinting of vitreous may not always be informative with respect to metabolic activity in the retina. However, in some pathological states where there is increased permeability of the retinal vessels or RPE, vitreous analysis may be of value. This study provides a guide to the classes of common metabolites that can be expected either exclusively or non-exclusively across different ocular tissues and serve as valuable baseline knowledge to future studies. For example, one of the common metabolites detected in both the retina and vitreous only in our study was urate. Baban et al[39] found an increased in purine metabolism in the diabetic retina that corresponded to an increased vitreal urate level. We also know from our study that urate can be detected in the vitreous. Hence, studies looking at vitreal urate level will always need to include a control group to measure differences in concentration. On the other hand,

we know that vitreous sample would not be a good surrogate in studies looking at certain metabolites that were found exclusively identified in the retina (ie. Retinal palmitate, an antioxidant), in physiological states at least.

In conclusion, applying metabolomics to ocular tissues is likely to become an increasingly important technique for studying diseases of the eye, identifying biomarkers and investigating the effects of therapeutic interventions. However, caution must be applied when assuming that sampling of ocular biofluids will give insights into the metabolome of adjacent tissue structures. When analysing the metabolome of ocular tissue post-mortem, it is important to recognise that there are time-dependent post-mortem changes, which will make it challenging to use human tissue, although if stringent methodologies are applied, metabolomics could be a very valuable approach in animal models.

Abbreviations

ARVO- Association for Research in Vision and Ophthalmology; FDR-False Discovery Rate; GC-MS-Gas Chromatography-Mass Spectrometry; NetCDF- Network Common Data Form; PCA-Principal Components Analysis; QC-Quality Control; UHPLC-MS-Ultra High Performance Liquid Chromatography-Mass Spectrometry

Acknowledgement

The authors would like to thank Dr Paul Begley from Centre for Advanced Discovery and Experimental Therapeutics, Manchester, for his technical support in the GC-MS analysis. We would also like to thank the Manchester Biomedical Research Centre for supporting this research.

Financial Disclosures: No financial disclosures

References

1. Dunn WB, Broadhurst DI, Atherton HJ, Goodacre R, Griffin JL. Systems level studies of mammalian metabolomes: the roles of mass spectrometry and nuclear magnetic resonance spectroscopy. *Chem Soc Rev* 2011; **40**(1)**:** 387-426.

2. Psychogios N, Hau DD, Peng J, Guo AC, Mandal R, Bouatra S *et al.* The human serum metabolome. *PLoS One* 2011; **6**(2)**:** e16957.

3. Bouatra S, Aziat F, Mandal R, Guo AC, Wilson MR, Knox C *et al.* The human urine metabolome. *PLoS One* 2013; **8**(9)**:** e73076.

4. Kell DB. Metabolomics and systems biology: making sense of the soup. *Curr Opin Microbiol* 2004; **7**(3)**:** 296-307.

5. Raamsdonk LM, Teusink B, Broadhurst D, Zhang N, Hayes A, Walsh MC *et al.* A functional genomics strategy that uses metabolome data to reveal the phenotype of silent mutations. *Nat Biotechnol* 2001; **19**(1)**:** 45-50.

6. Chen L, Zhou L, Chan EC, Neo J, Beuerman RW. Characterization of the human tear metabolome by LC-MS/MS. *J Proteome Res* 2011; **10**(10)**:** 4876-4882.

7. Locci E, Scano P, Rosa MF, Nioi M, Noto A, Atzori L *et al.* A metabolomic approach to animal vitreous humor topographical composition: a pilot study. *PLoS One* 2014; **9**(5)**:** e97773.

8. Yanshole VV, Snytnikova OA, Kiryutin AS, Yanshole LV, Sagdeev RZ, Tsentalovich YP. Metabolomics of the rat lens: a combined LC-MS and NMR study. *Exp Eye Res* 2014; **125:** 71-78.

9. Mains J, Tan LE, Zhang T, Young L, Shi R, Wilson C. Species variation in small molecule components of animal vitreous. *Invest Ophthalmol Vis Sci* 2012.

10. Sun N, Ly A, Meding S, Witting M, Hauck SM, Ueffing M *et al.* High-resolution metabolite imaging of light and dark treated retina using MALDI-FTICR mass spectrometry. *Proteomics* 2014; **14**(7-8)**:** 913-923.

11. Mayordomo-Febrer A, López-Murcia M, Morales-Tatay JM, Monleón-Salvado D, Pinazo-Durán MD. Metabolomics of the aqueous humor in the rat glaucoma model induced by a series of intracamerular sodium hyaluronate injection. *Exp Eye Res* 2015; **131:** 84-92.

12. Du J, Cleghorn WM, Contreras L, Lindsay K, Rountree AM, Chertov AO *et al.* Inhibition of mitochondrial pyruvate transport by zaprinast causes massive accumulation of aspartate at the expense of glutamate in the retina. *J Biol Chem* 2013; **288**(50)**:** 36129-36140.

13. Kryczka T, Ehlers N, Nielsen K, Midelfart A. Impact of organ culturing on metabolic profile of human corneas: preliminary results. *Acta Ophthalmol* 2012; **90**(8)**:** 761-767.

14. Song Z, Gao H, Liu H, Sun X. Metabolomics of rabbit aqueous humor after administration of glucocorticosteroid. *Curr Eye Res* 2011; **36**(6)**:** 563-570.

15. Young SP, Nessim M, Falciani F, Trevino V, Banerjee SP, Scott RA *et al.* Metabolomic analysis of human vitreous humor differentiates ocular inflammatory disease. *Mol Vis* 2009; **15:** 1210-1217.

16. Kryczka T, Szaflik JP, Szaflik J, Midelfart A. Influence of donor age, post-mortem time and cold storage on metabolic profile of human cornea. *Acta Ophthalmol* 2013; **91**(1)**:** 83-87.

17. Boulagnon C, Garnotel R, Fornes P, Gillery P. Post-mortem biochemistry of vitreous humor and glucose metabolism: an update. *Clin Chem Lab Med* 2011; **49**(8)**:** 1265-1270.

18. Dunn WB, Broadhurst D, Begley P, Zelena E, Francis-McIntyre S, Anderson N *et al.* Procedures for large-scale metabolic profiling of serum and plasma using gas chromatography and liquid chromatography coupled to mass spectrometry. *Nat Protoc* 2011; **6**(7)**:** 1060-1083.

19. Smith CA, Want EJ, O'Maille G, Abagyan R, Siuzdak G. XCMS: processing mass spectrometry data for metabolite profiling using nonlinear peak alignment, matching, and identification. *Anal Chem* 2006; **78**(3)**:** 779-787.

20. Dunn WB, Broadhurst D, Brown M, Baker PN, Redman CWG, Kenny LC *et al.* Metabolic profiling of serum using Ultra Performance Liquid Chromatography and the LTQ-Orbitrap mass spectrometry system. *Journal of Chromatography B-Analytical Technologies in the Biomedical and Life Sciences* 2008; **871**(2)**:** 288-298.

21. Brown M, Wedge DC, Goodacre R, Kell DB, Baker PN, Kenny LC *et al.* Automated workflows for accurate mass-based putative metabolite identification in LC/MS-derived metabolomic datasets. *Bioinformatics* 2011; **27**(8)**:** 1108-1112.

22. Sumner LW, Amberg A, Barrett D, Beale MH, Beger R, Daykin CA *et al.* Proposed minimum reporting standards for chemical analysis. *Metabolomics* 2007; **3**(3)**:** 211-221.

23. Xia J, Sinelnikov IV, Han B, Wishart DS. MetaboAnalyst 3.0-making metabolomics more meaningful. *Nucleic Acids Res* 2015; **43**(W1)**:** W251-257.

24. Benjamini Y, Hochberg Y. Controlling the false discovery rate: a practical and powerful approach to multiple testing. *Journal of the Royal Statistical Society, Series B*

1995; **57**(1)**:** 289–300.

25. Chinopoulos C. Which way does the citric acid cycle turn during hypoxia? The critical role of α-ketoglutarate dehydrogenase complex. *J Neurosci Res* 2013; **91**(8)**:** 1030-1043.

26. Brekke E, Walls AB, Nørfeldt L, Schousboe A, Waagepetersen HS, Sonnewald U. Direct measurement of backflux between oxaloacetate and fumarate following pyruvate carboxylation. *Glia* 2012; **60**(1)**:** 147-158.

27. Sonnewald U, Westergaard N, Hassel B, Müller TB, Unsgård G, Fonnum F *et al.* NMR spectroscopic studies of 13C acetate and 13C glucose metabolism in neocortical astrocytes: evidence for mitochondrial heterogeneity. *Dev Neurosci* 1993; **15**(3-5)**:** 351-358.

28. Pisarenko O, Studneva I, Khlopkov V, Solomatina E, Ruuge E. An assessment of anaerobic metabolism during ischemia and reperfusion in isolated guinea pig heart. *Biochim Biophys Acta* 1988; **934**(1)**:** 55-63.

29. Des Rosiers C, Di Donato L, Comte B, Laplante A, Marcoux C, David F *et al.* Isotopomer analysis of citric acid cycle and gluconeogenesis in rat liver. Reversibility of isocitrate dehydrogenase and involvement of ATP-citrate lyase in gluconeogenesis. *J Biol Chem* 1995; **270**(17)**:** 10027-10036.

30. Des Rosiers C, Fernandez CA, David F, Brunengraber H. Reversibility of the mitochondrial isocitrate dehydrogenase reaction in the perfused rat liver. Evidence from isotopomer analysis of citric acid cycle intermediates. *J Biol Chem* 1994; **269**(44)**:** 27179-27182.

31. Schmidt SY, Berson EL. Postmortem metabolic capacity of photoreceptor cells in human and rat retinas. *Invest Ophthalmol Vis Sci* 1980; **19**(11)**:** 1274-1280.

32. JM B, JL T, L S *Biochemistry*, 5th edn. W. H. Freeman and Company: New York; 2002.

33. Chao XD, Fei F, Fei Z. The role of excitatory amino acid transporters in cerebral ischemia. *Neurochem Res* 2010; **35**(8)**:** 1224-1230.

34. Benveniste H, Drejer J, Schousboe A, Diemer NH. Elevation of the extracellular concentrations of glutamate and aspartate in rat hippocampus during transient cerebral ischemia monitored by intracerebral microdialysis. *J Neurochem* 1984; **43**(5)**:** 1369-1374.

35. Dreyer EB, Zurakowski D, Schumer RA, Podos SM, Lipton SA. Elevated glutamate levels in the vitreous body of humans and monkeys with glaucoma. *Arch Ophthalmol* 1996; **114**(3)**:** 299-305.

36. Gardiner EE, Newberry RC, Keng JY. Postmortem time and storage temperature affect the concentrations of hypoxanthine, other purines, pyrimidines, and nucleosides in avian and porcine vitreous humor. *Pediatr Res* 1989; **26**(6)**:** 639-642.

37. Forrester J DA, McMenamin P, Roberts F *The Eye. Basic sciences in practice.*, 3rd edn. Elsevier; 2008.

38. Cunha-Vaz JG, Maurice DM. The active transport of fluorescein by the retinal vessels and the retina. *J Physiol* 1967; **191**(3)**:** 467-486.

39. B B, F L, A M, Gi P, S S, G R *et al.* Increased in purine metabolism in the human diabetic retina indicates monosodium urate (MSU)-mediated inflammatory effects in diabetic retinopathy. *Investigative ophthalmology and visual science* 2014; **55**(13).

Table 1: List of metabolite features identified by GC-MS that have changed significantly over 48 hours post-mortem period and its direction of change, indicated by median of its relative concentration at 0 hour over 48 hours.

Table 2: List of metabolites detected across different ocular tissues using the GC-MS.

Figure 1. PCA scores plot for data acquired for the retina by GC-MS showing partial or complete separation of samples collected 8, 24 and 48 hours post-mortem after storage at 4^{o}C. Red circle = retina extracted after 0 hours storage; green circle = retina extracted after 2 hours storage; dark blue circle = retina extracted after 4 hours storage; cyan circle =
retina extracted after 8 hours storage; pink circle = retina extracted after 24 hours storage; yellow circle = retina extracted after 48 hours storage; grey circle = quality control sample (QC).

Figure 2. PCA scores plot for data acquired for the retina applying (a) positive ion UHPLC-MS and (b) negative ion UHPLC-MS showing partial or complete separation of samples collected 8, 24 and 48 hours post-mortem after storage at 4^{o}C. Red circle = retina extracted after 0 hours storage; green circle = retina extracted after 2 hours storage; dark blue circle = retina extracted after 4 hours storage; cyan circle =retina extracted after 8 hours storage; pink circle = retina extracted after 24 hours storage; yellow circle = retina extracted after 48 hours storage; grey circle = quality control sample (QC).

Figure 3. Box and whisker plots showing changes in metabolite concentrations over a 48 h period for (a) malic acid, (b) ascorbic acid, (c) octadecatrienoic carnitine and (d) PC(40:4)

Figure 4. Venn diagram showing the number of unique metabolite detected across different ocular tissues (cornea, vitreous, retina, lens) by (a) GC-MS and (b) UHPLC-MS

Figure 1. PCA scores plot for data acquired for the retina by GC-MS showing partial or complete separation of samples collected 8, 24 and 48 hours post-mortem after storage at 4^{o}C. Red circle = retina extracted after 0 hours storage; green circle = retina extracted after 2 hours storage; dark blue circle = retina extracted after 4 hours storage; cyan circle =
retina extracted after 8 hours storage; pink circle = retina extracted after 24 hours storage; yellow circle = retina extracted after 48 hours storage; grey circle = quality control sample (QC).

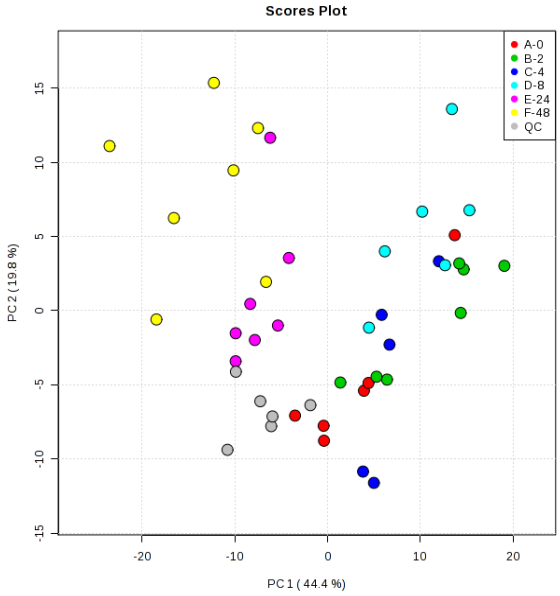

Figure 2. PCA scores plot for data acquired for the retina applying (a) positive ion UHPLC-MS and (b) negative ion UHPLC-MS showing partial or complete separation of samples collected 8, 24 and 48 hours post-mortem after storage at 4^{o}C. Red circle = retina extracted after 0 hours storage; green circle = retina extracted after 2 hours storage; dark blue circle = retina extracted after 4 hours storage; cyan circle =retina extracted after 8 hours storage; pink circle = retina extracted after 24 hours storage; yellow circle = retina extracted after 48 hours storage; grey circle = quality control sample (QC).

(a)

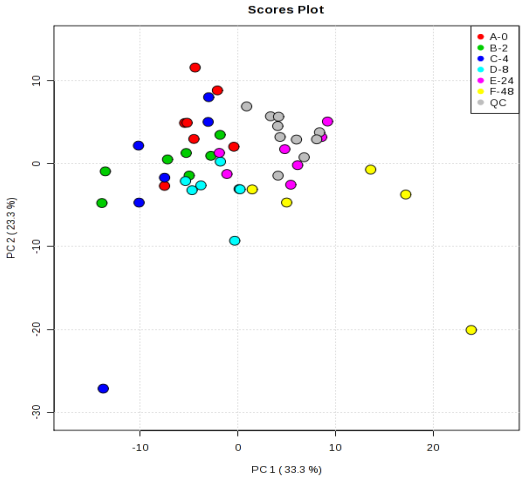

(b)

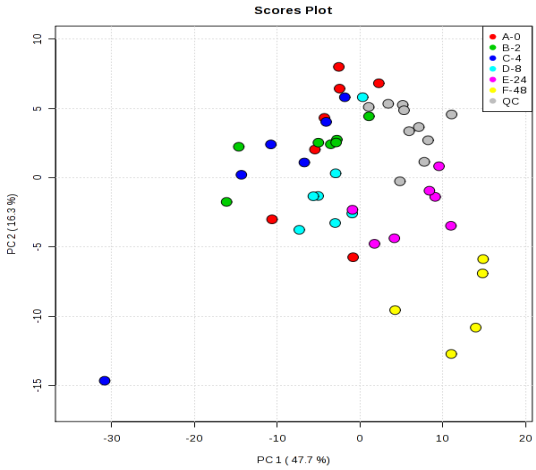

Figure 3. Box and whisker plots showing changes in metabolite concentrations over a 48 h period for (a) malic acid, (b) ascorbic acid, (c) octadecatrienoic carnitine and (d) phosphatidylcholine (40:4)

(a)

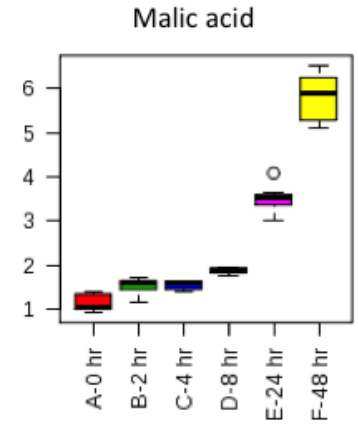

(b)

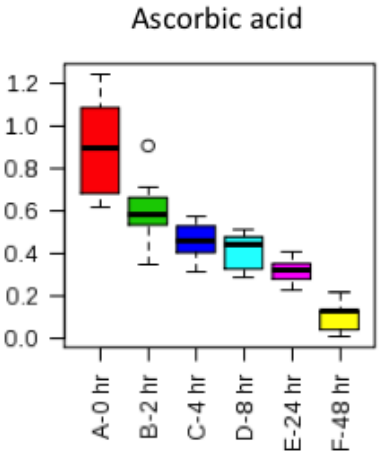

(c)

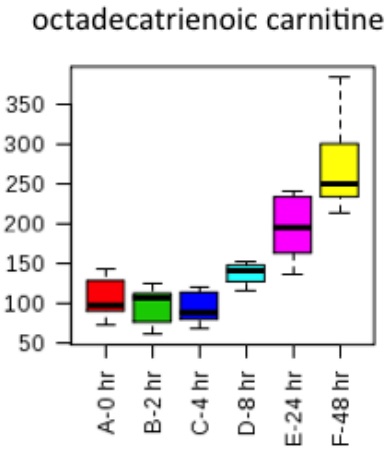

(d)

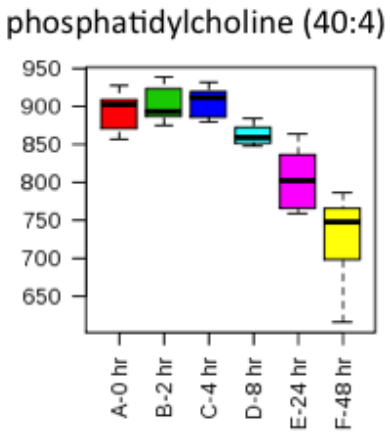
phosphatidylcholine (40:4)
950
900
850
800
750
700
650
A-0 hr
B-2 hr
C-4 hr
D-8 hr
E-24 hr
F-48 hr

Figure 4. Venn diagram showing the number of unique metabolite detected across different ocular tissues (cornea, vitreous, retina, lens) by (a) GC-MS and (b) UHPLC-MS

(a)

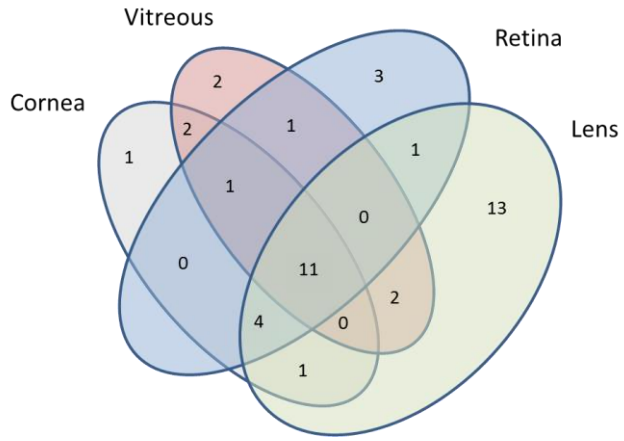

(b)

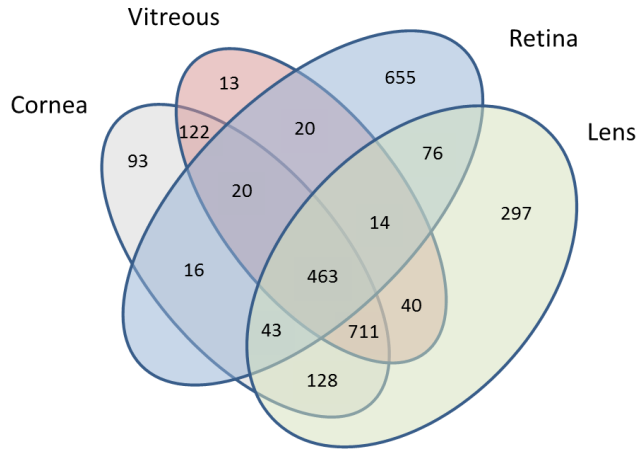

Table 1: List of metabolite features identified by GC-MS that have changed significantly over 48 hours post-mortem period and its direction of change, indicated by median of its relative concentration at 0 hour over 48 hours.

Metabolite	Time point where statistically significant changes in concentration were first observed (hours)	Median(0 hours) /Median(48 hours)
Leucine	48	0.452
Glycerol	24	2.453
Uracil	24	0.128
Malic acid	2	0.243
Methionine	24	0.236
Creatinine	2	1.551
Glutamic acid	8	1.352
Phenylalanine	24	0.283
Citric acid	2	0.404
Tetradecanoic acid	24	1.822
Ascorbic acid	48	7.900
Hexadecanoic acid	8	1.609
Heptadecanoic acid	24	2.319
Stearic acid	24	1.740
Tryptophan	48	0.089
Arachidic Acid	24	1.592

Table 2: List of metabolites detected across different ocular tissues using the GC-MS.

Metabolite	Sample type in which metabolite was detected
Arachidic Acid	Cornea
4-hydroxyproline	Lens
Adenosine-5-monophosphate	Lens
Cysteine	Lens
glycerol-3-phosphate	Lens
Leucine	Lens
Mannitol	Lens
N-formylmethionine	Lens
Pentanedioic acid, 2-hydroxy	Lens
Ribitol	Lens
Scyllo-inositol	Lens
Threitol	Lens
Tolnaftate	Lens
Valine	Lens
Butanoic acid	Retina
Citric acid	Retina
Serine	Retina
4-aminobutyric acid	Vitreous
Benzoic acid	Vitreous
1-Iodo-2-methylundecane	Cornea and vitreous
Glucose	Cornea and vitreous
glycerol	Lens and cornea
Tyrosine	Lens and retina
5,5-dithiobis-(2-nitrobenzoic acid)	Lens and vitreous
Threonic acid	Lens and vitreous
Tetradecanoic acid	Vitreous and retina
Creatinine	Cornea, retina and vitreous
Aspartic acid	Lens, cornea and retina
Glycine	Lens, cornea and retina
Phenylalanine	Lens, cornea and retina
Propanoic acid, 2-hydroxy	Lens, cornea and retina
Butane, 1,4-dibromo-	Lens, cornea, vitreous and retina
Butanedioic acid	Lens, cornea, vitreous and retina
Hexadecanoic acid	Lens, cornea, vitreous and retina
Lactic acid	Lens, cornea, vitreous and retina
Malic acid	Lens, cornea, vitreous and retina
myo-Inositol	Lens, cornea, vitreous and retina
phosphate	Lens, cornea, vitreous and retina
Pyroglutamic acid	Lens, cornea, vitreous and retina
Stearic acid	Lens, cornea, vitreous and retina
Threonine	Lens, cornea, vitreous and retina
Urea	Lens, cornea, vitreous and retina